Pharm Res (2010) 27:1644–1658
DOI 10.1007/s11095-010-0150-6

RESEARCH PAPER

In Situ Artificial Membrane Permeation Assay under Hydrodynamic Control: Permeability-pH Profiles of Warfarin and Verapamil

Matěj Velický • Dan F. Bradley • Kin Y. Tam • Robert A. W. Dryfe

Received: 25 January 2010 / Accepted: 1 April 2010 / Published online: 7 May 2010

ABSTRACT

Purpose To investigate the permeation of two ionisable drug molecules, warfarin and verapamil, across artificial membranes. For the first time since the introduction of the parallel artificial membrane permeation assay (PAMPA) in 1998, *in situ* permeation-time profiles of drug molecules are studied.

Methods The method employs a rotating-diffusion cell where the donor and acceptor compartments are separated by a lipid-impregnated artificial membrane. The permeation of the solute is investigated under well-defined hydrodynamic conditions with control over the unstirred water layer. The flux of the permeating molecule is analysed *in situ* using UV spectrophotometry.

Results *In situ* permeation-time profiles are obtained under hydrodynamic control and used to determine permeability coefficients. An advanced analytical transport model is derived to account for the membrane retention, two-way flux and pH gradient between the two compartments. Moreover, a numerical permeation model was developed to rationalise the time-dependent permeation profiles. The membrane permeability, intrinsic permeability and unstirred water permeability coefficients of two drug molecules are obtained from two independent methods, hydrodynamic extrapolation and pH profiling, and the results are compared.

Conclusions Both warfarin and verapamil exhibit high permeability values, which is consistent with the high fraction absorbed in human. Our results demonstrate that a considerable lag-time, varying with the solute lipophilicity and stirring rate, exists in membrane permeation and leads to incorrect compound ranking if it is not treated properly. Comparison of the permeability data as a function of pH and stirring rate suggests that some transport of the ionized molecules occurs, most likely via ion-pairing.

KEY WORDS hydrodynamic control · in situ permeation · PAMPA · permeability · unstirred water layer

ABBREVIATIONS AND SYMBOLS

A	membrane area
α	hydrodynamic exponent
BM-PAMPA	bio-mimetic PAMPA
$c(t)$	time-dependent solute concentration
Caco-2	colorectal adenocarcinoma cell epithelial line
CHES	2-(Cyclohexylamino)ethanesulfonic acid
D_{aq}	aqueous diffusion coefficient
D_m	membrane diffusion coefficient
DOPC	dioleoyl phosphatidylcholine
DOPC-PAMPA	dioleoyl phosphatidylcholine PAMPA
DS-PAMPA	double-sink PAMPA
f_n	neutral fraction of the solute
h	membrane thickness
HDM-PAMPA	hexadecane PAMPA
IAM	immobilised artificial membrane
$J(t)$	time-dependent solute flux
K_d	distribution coefficient

Electronic Supplementary Material The online version of this article (doi:10.1007/s11095-010-0150-6) contains supplementary material, which is available to authorized users.

M. Velický · D. F. Bradley · R. A. W. Dryfe (✉)
School of Chemistry, University of Manchester
Oxford Road
Manchester M13 9PL, UK
e-mail: robert.dryfe@manchester.ac.uk

K. Y. Tam (✉)
AstraZeneca, Mereside
Alderley Park, Macclesfield
Cheshire SK10 4TG, UK
email: kin.tam@astrazeneca.com

K_{OCT}	octanol/water distribution coefficient
MDCK	Madin-Darby canine kidney epithelial cell line
P	(not specified) permeability coefficient
P_0	intrinsic permeability coefficient
PAMPA	parallel artificial membrane permeation assay
P_e	effective (measured) permeability coefficient
P_m	membrane permeability coeffcient
PTFE	polytetrafluoroethylene
P_u	unstirred water layer permeability coefficient
PVDF	polyvinylidene fluoride
R	fractional membrane retention
t	time
UWL	unstirred water layer
V	volume
δ_{UWL}	unstirred water layer thickness
v	kinematic viscosity
τ_{LAG}	lag-time

All permeability coefficients are in units of cm s^{-1}

INTRODUCTION

In the last decade, the parallel artificial membrane permeation assay (PAMPA) has become a standard tool to predict human oral absorption of drug candidates in the early stages of the drug discovery pipeline. Although it is ideally suited only for transcellular absorption prediction, many advantages, such as high-throughput, low cost, and the possibility of pH profiling and stirring, over the conventional cell-based *in vitro* assays, such as Caco-2 (1, 2) and MDCK (3), have made PAMPA a widely used screening method (4–10). A number of groups have developed their own versions of PAMPA with the major difference being embedded in the membrane composition. The first immobilised artificial membrane (IAM) used in PAMPA consisted of egg-yolk lecithin in dodecane immobilised on a thin (100 μm) hydrophobic filter (10, 11). The next generation of IAMs used 2% weight synthetic dioleoyl phosphatidylcholine in *n*-dodecane (DOPC-PAMPA) (12). This assay was a predecessor of a more advanced model called Double-Sink method (DS-PAMPA) introduced by Avdeef *et al.* (8, 9, 13). DS-PAMPA combines a pH gradient between the donor and acceptor solution (usually 5.0–7.4 and 7.4, respectively) and addition of chemical scavengers to the acceptor to mimic the presence of serum proteins in blood. This results in double-sink conditions that suppress the back-flux permeation from the acceptor to donor compartment and shorten the experimental time. A further advantage of this PAMPA version is the introduction of individual well stirring that enables the unstirred water layer (UWL) to be controlled on an empirical basis (14). However, one drawback of this method is the high lipid content (20% by weight lecithin in dodecane) causing undesirably high membrane retention of lipophilic drugs. Sugano *et al.* used a mixture of various lipids dissolved in 1,7-octadiene to mimic the content of mammalian cell walls in a so-called 'bio-mimetic' PAMPA (BM-PAMPA) (15), which gave an excellent prediction of the passive intestinal absorption in combination with a paracellular pathway model based on the Renkin function (16, 17). Faller *et al.* introduced a version based on hexadecane, immobilized on a thin (10 μm) polycarbonate filter of low porosity, in order to resemble better the thickness of bi-layer membranes found in living cells (HDM-PAMPA) (18). This group also used the PAMPA method for the high-throughput measurement of octanol/water partition coefficients (19). More membrane models, such as lipid-oil-lipid tri-layer membranes (20), liposome-based membranes (21–23), blood-brain barrier mimics (24) and other approaches to permeability measurement (25, 26), or prediction of passive intestinal absorption (27) have been reported in the last decade. Also, the effect of lipid composition on permeability was investigated, based on a liposome permeation study (28).

Despite the rapid development of PAMPA since 1998, there are some issues that have been rarely, if at all, addressed in literature. First of all, many researchers still use inadequate analytical transport models to interpret their data. With increasing complexity of the assay, such as pH-gradient introduction, stirring, membrane retention, membrane saturation lag-time, serum protein or precipitate presence, more advanced transport models need to be considered. An extensive list of the various transport models can be found in a previous publication (8). Another issue is the ex situ analysis of the acceptor and donor wells and consequent single time-point data processing. Finally, the stirring of the aqueous phase has a profound effect on the permeability measurement and analysis.

Although the importance of stirring in permeability studies has been shown before (13, 14, 29–31), most researchers still follow the unstirred version of PAMPA. The unstirred water layer adjacent to the membrane is a region where the concentration of the permeating compound is governed solely by diffusion. Some reports claim this layer could be as thick as 1.5–4.0 mm in the case of highly lipophilic/permeable molecules (14). Since the UWL thickness in the human small intestine is assumed to be 30–100 μm (32), the unstirred permeation assay does not match *in vivo* conditions correctly. As a consequence, the permeability of highly lipophilic drugs is underestimated due to the large UWL resistance hindering the permeation in the *in vitro* assay (e.g. verapamil, see below). Such underestimated permeability values do not give any

information about the drug-membrane interactions and are not suitable for ranking of drug candidates within a specific membrane model. Moreover, the UWL affects the permeation to different extents, depending on the aqueous pH. In this report, we present a hydrodynamically controlled artificial membrane permeation study of two widely available drugs, warfarin (weak acid) and verapamil (weak base). The physicochemical and bio-relevant properties of these drugs are listed in Table 1.

We introduce an *in situ* UV spectrophotometry measurement resulting in an absorbance/concentration-time profile. For that reason, we have derived an analytical model to determine the effective permeability coefficient, P_e, using least-square analysis of these time profiles. The analytical model accounts for the following permeation attributes: pH-gradient between donor and acceptor compartments, membrane retention, membrane saturation lag-time period and stirring.

The basic experimental method recently introduced by this group (33) was further developed into a single-permeation channel measurement designed to investigate physicochemical aspects of the drug permeation. It employs *in situ* UV measurement of the solute combined with stirring of both acceptor and donor compartments in a system with defined symmetric geometry. The acceptor pH is kept at 7.4; the donor pH is varied between 3.0 and 10.0. The standard permeation time is as short as 20–30 min, and stirring rates in the range of 200–1500 rpm are used (see Fig. 1 for the experimental schematic). The chosen membrane model comprised 1.5% weight of dioleoyl phosphatidylcholine and 0.5% weight stearic acid dissolved in 1,9-decadiene and immobilised on a hydrophobic polyvinylidene fluoride (PVDF) filter. The solvent, 1,9-decadiene, is not too volatile, relatively safe to work with, and appears to have suitable biological relevance (34).

The purpose of this study was, therefore, to examine drug permeation under controlled hydrodynamic conditions and to investigate the time-dependent flux of the compound observed *in situ*. We have been able to measure directly effective permeability coefficients as high as 4300×10^{-6} cm s^{-1} and as low as 5×10^{-6} cm s^{-1} under stirred conditions. Permeability measurements of ionisable drug compounds as a function of pH along with permeability dependence on stirring rate give two different approaches for the determination of the membrane permeability, intrinsic permeability and unstirred water layer permeability. It is noted that the membrane/intrinsic permeabilities are important transport parameters describing the interaction between the drug and membrane barrier. Furthermore, a numerical permeation model was developed to support experimental results.

MATERIALS AND METHODS

Materials

Sodium phosphate (98.5%), CHES buffer (2-(Cyclohexylamino)ethanesulfonic acid 99%), buffer solutions for pH meter calibration (pH 4.00, 7.00, 10.0), 1,9-decadiene (96%), DOPC (1,2-Dioleoyl-*sn*-glycero-3-phosphocholine, approx 99%), stearic acid (grade I approx 99%), warfarin (4-Hydroxy-3-(3-oxo-1-phenylbutyl)coumarin, min 98%), (±)-verapamil hydrochloride (5-[*N*-(3,4-Dimethoxyphenylethyl)methylamino]-2-(3,4-dimethoxyphenyl)-2-isopropylvaleronitrile hydrochloride, min 99%) were purchased from Sigma-Aldrich. Sodium hydroxide (98.8%) and sulfuric acid (98%) were used for pH adjustment (Fisher Scientific UK Ltd.). Sodium acetate (98%) was purchased from BDH Ltd. Precision-ground glass tubes, which served as the donor compartment, were obtained from Glass Precision Engineering Ltd. (Leighton Buzzard, UK), "Durapore"® PVDF hydrophobic membrane filters (0.45 μm pore size, 125 μm thickness, 75% porosity, 13 mm diameter) supplied by Millipore, were attached to the glass tubes using Araldite Rapid glue (Bostik Ltd). and cut to fit the tube outer diameter after a few hours of drying (acceptor-side membrane area = 1.04 cm^2, donor-side membrane area = 0.79 cm^2). Water of 18.2 MΩ cm resistivity purified by a "PURELAB" ultrafiltration unit (ELGA) was used in solution preparation. Flexible plastic foil (Parafilm, Pechiney Plastic Packaging) was used to wrap the top of the donor compartment in unstirred permeation experiments.

Table I Physicochemical and bio-relevant properties of warfarin and verapamil

	MW / $gmol^{-1}$ [a]	%HA [b]	pK_a [c]	log K_{OCT} (7.4) [c]	D_{aq} / $10^{-6}cm^2s^{-1}$ [d]
Warfarin	308.33	93	4.82	1.12	4.32
Verapamil	454.60	84	9.07	2.51	3.57

[a] Values from chemicals supplier

[b] Human absorption values cited from (46) and corrected for the first-pass hepatic clearance based on the data published in (47)

[c] Values cited from (8)

[d] Aqueous diffusion coefficients calculated using Eq. 4 in ref. (6)

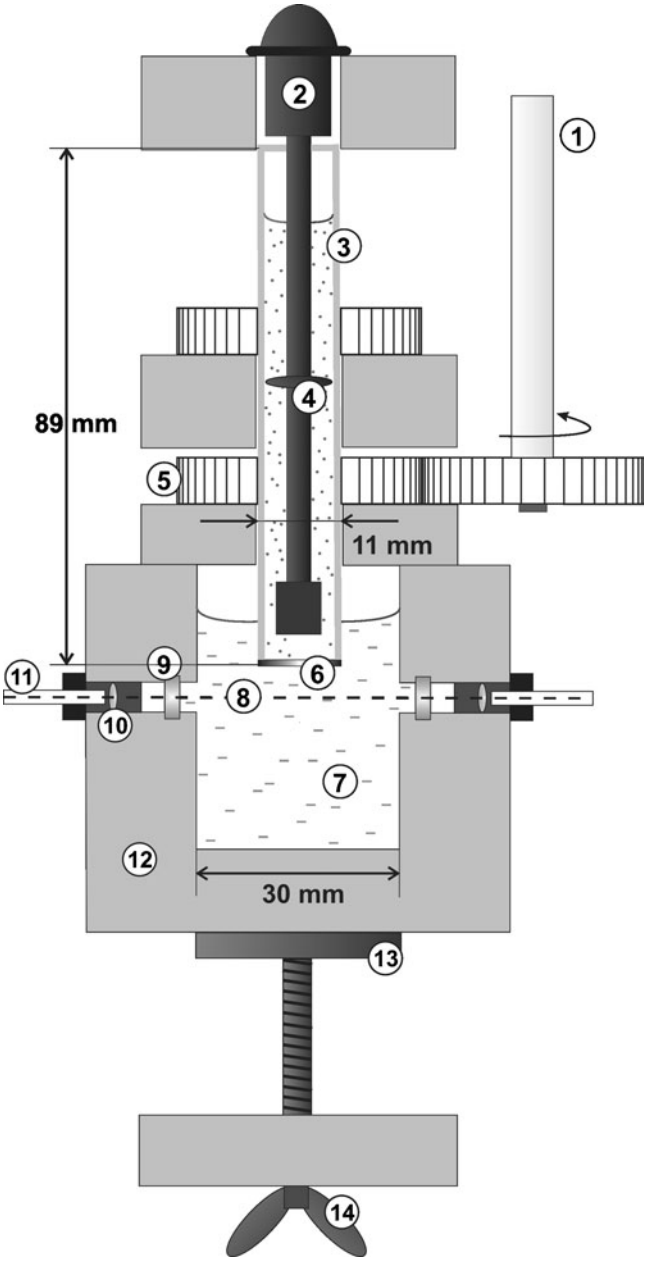

Fig. 1 Schematic diagram of the permeation cell used for *in situ* UV measurement: 1, rotation controller; 2, paddle; 3, glass tube (donor compartment); 4, spacer disc; 5, PTFE cogwheel tightly connected to the glass tube; 6, PVDF membrane; 7, acceptor solution; 8, UV source optical path; 9, quartz window; 10, quartz lens; 11, fiber-optic cable; 12, PTFE acceptor cell; 13, steel pad; 14, steel pad screw.

Solution pH was measured using a HI991300 pH meter (Hanna Instruments). UV spectra were acquired using a DH-2000-BAL spectrometer equipped with a DH-2000-BD deuterium bulb and fiber-optic cable (supplied by Ocean Optics, the Netherlands) and controlled using a USB2000 interface (Micropack GmbH). Rotation of the donor compartment was controlled using a Model 616 rotating-disc controller (EG&G Parc). The permeation cell, consisting of an acceptor compartment made of polytetrafluoroethylene (PTFE), equipment stand and other accessories (Fig. 1) was made in-house. The numerical permeation model was developed using Comsol "Multiphysics" software (Comsol UK, Hatfield, UK). Simulations were executed on a desktop PC; however, the geometric dimensions of the model also presented a challenge in terms of memory allocation: to maintain the mesh quality of the precursor models required nearly 45,000 elements per build. This led to a run time of 5–15 min per model run. The number of stored solutions also needed to be kept to <150 per run, otherwise the model would crash due to lack of memory.

Artificial Membrane Permeation Assay under Hydrodynamic Control

UV Calibration in the Acceptor Compartment

The optical path of the PTFE acceptor compartment was measured to be 32.5±0.5 mm. To avoid uncertainty in the optical path length, the composite parameter $\varepsilon \cdot l$ (ε—molar extinction coefficient, l—optical path length) was found when calculating the concentration from the absorbance. Absorption spectra of the two studied drug molecules in 10 mM sodium phosphate solution within the range of absorption (200–400 nm) can be found in the Supplementary Material.

Permeation Cell Assembly

The PTFE acceptor compartment was filled with 20 ml of 10 mM sodium phosphate buffer solution at pH=7.4. A PVDF filter of apparent area 0.68 cm^2 (average of donor and acceptor side multiplied by filter porosity) attached to the donor glass tube was soaked with 14 µl of a 1,9-decadiene solution containing 1.5% weight DOPC and 0.5 % weight stearic acid. The tube was gently shaken for a few seconds, and the excess solvent (ca 2 µl) removed by gentle wiping with tissue paper. Subsequently, a set volume (3–5 ml) of 10 mM buffer solution containing the drug molecule at a given pH was dispensed into the donor tube. Sodium acetate (pH 3.5–5.5), sodium phosphate (pH 6.0–8.5) and CHES buffer (pH 8.5–10.0) were used as the donor phase buffers. The drug concentration in the donor solution was varied according to its solubility and the assay requirements (7–300 µM). The buffer concentration was sufficiently high to ensure that the change in drug concentration was always less than 1% of the buffer concentration (to maintain a constant pH). After dispensing the donor solution, the tube was placed in a cogwheel, and a plastic paddle was fitted into the tube. The paddle, which was used to control the stirring conditions on the donor

side, was stationary during the experiment. Then the acceptor compartment was attached and fixed using a screwed pad and equipped with the fiber-optic cable. Finally, the rotation controller was attached to a PTFE cogwheel, tightly embracing the donor tube. For the detailed cell design and its dimensions, see Fig. 1.

In Situ UV Spectra Time Acquisition in the Acceptor Compartment

After assembly of the cell, the reference and dark spectra of the acceptor solution were taken. Stirring and spectral time acquisition were started simultaneously. Four different wavelength channels at the spectral peak maxima plus one background channel were recorded for permeation times of 20–30 min. A typical spectral acquisition frequency was 1 s^{-1}. At the end of the permeation, the whole spectrum was taken as a comparison to the calibration spectrum. Permeation was conducted at ambient temperature, 21.8± 0.3°C (mean ± standard deviation over 50 temperature measurements, measured during each experimental session). There are many other parameters with profound effect on permeation, such as choice of the membrane filter, solvent, lipid content or presence of co-solvents in the aqueous phase. Choosing an ambient temperature has the advantage of being close to pK_a measurement standards (25°C). The permeation assay under stationary conditions was conducted in the same permeation cell using a single-time data point (at $t \sim$ 18–24 h).

Permeation Cell Disassembly and Donor Compartment Ex Situ Analysis

The permeation cell was disassembled, and samples from the donor compartment were taken for later analysis. The acceptor compartment solution pH was checked in every third permeation experiment and found not to change by more than 0.1 pH units. The whole spectrum and individual wavelength channels of the diluted donor solution were recorded along with the original donor solution sample.

Single pH Point Data Generation

A permeation data set for a given donor pH / acceptor pH 7.4 was obtained as follows. The whole permeation data set (i.e. stirring rates 200, 250, 290, 400, 600, 1000 and 1500 rpm, corresponding to angular velocities of 21, 26, 30, 42, 63, 105 and 157 rad s^{-1}) was obtained in a single experimental day using the same solutions and pH calibration/adjustment. This procedure was performed three times to reduce the experimental error. Experiments investigating the membrane stability at different stirring rates and effectiveness of stirring to induce sufficient mixing are discussed in the Supplementary Material.

Permeation Data Analysis

The raw absorbance data were corrected for any background contribution by subtracting the background channel absorbance. Then the absorbance was converted to the concentration-time profiles (based on the solute Beer-Lambert calibration) and further to ln(k) *vs.* time plots (see next section). From the slope of these functions, the effective permeability (P_e) was calculated. Four wavelength channels were analysed in this way separately and, depending on the data quality, were averaged to produce the effective permeability value.

Shake-Flask Method

The standard shake-flask method was employed to determine the membrane-donor phase distribution coefficient. The lipid solution of 1.5% weight DOPC and 0.5 % weight stearic acid in 1,9-decadiene was shaken with a buffer solution containing the drug molecule and left still for 24 h. The drug concentrations in the aqueous phase before and after shaking were measured using UV absorbance spectroscopy, and the distribution coefficient, K_d, was determined using following equation:

$$K_d = \frac{V_{aq}}{V_{org}} \frac{\left(c_{aq}^{0} - c_{aq}^{eq}\right)}{c_{aq}^{eq}} \quad (1)$$

where V_{aq} and V_{org} are the volumes of the aqueous and organic phase, respectively, and c_{aq}^{0} and c_{aq}^{eq} are the aqueous drug concentrations before and after shaking, respectively.

Analytical Transport Model

Analytical Model Derivation

Various transport models with different limitations towards membrane retention, gradient pH, back-flux, lag-time or surfactants have been summarised by Avdeef (8). In order to interpret the data correctly, an advanced transport model that has been rarely used in PAMPA literature is presented herein. The model considers the pH gradient between the donor and acceptor compartment (possible back-flux from the acceptor to the donor), takes the membrane retention into account (fraction of the drug molecule retained within the membrane) and corrects for the initial lag-time, τ_{LAG}, (steady-state establishment across the membrane). Correction for the lag-time is important, as the neglect of this factor leads to the permeability of lipophilic molecules being under-

estimated, as discussed below. The distribution of the drug in the donor-membrane-acceptor system is depicted in Fig. 2 for an (a) ideally stirred and (b) unstirred system. Both cases assume time $>\tau_{\mathrm{LAG}}$ and therefore linear concentration distribution within the membrane. Fick's first law will apply for the permeation/diffusion in such a case.

The following relationships were used in the model derivation:

(i) Fick's first law applied to a homogeneous membrane:

$$\mathcal{J}(t) = P_{\mathrm{e}}^{\mathrm{D}\to\mathrm{A}} c_{\mathrm{D}}(t) - P_{\mathrm{e}}^{\mathrm{A}\to\mathrm{D}} c_{\mathrm{A}}(t) \tag{2}$$

where $\mathcal{J}(t)$ is the time-dependent flux of the solute across the membrane, $P_e^{\mathrm{D}\to\mathrm{A}}$ and $P_e^{\mathrm{A}\to\mathrm{D}}$ denote the effective permeability coefficients for the donor-to-acceptor and acceptor-to-donor transport, respectively. $P_{\mathrm{e}}^{\mathrm{A}\to\mathrm{D}}$represents the back-flux (acceptor-to-donor) transport that is usually neglected in PAMPA studies. Finally, $c_{\mathrm{D}}(t)$ and $c_{\mathrm{A}}(t)$ are the time-dependent bulk concentrations of the solute in the donor and acceptor compartment, respectively. Note that by the effective permeability coefficient, P_{e}, we usually mean the donor-to-acceptor effective permeability coefficient, $P_{\mathrm{e}}^{\mathrm{D}\to\mathrm{A}}$.

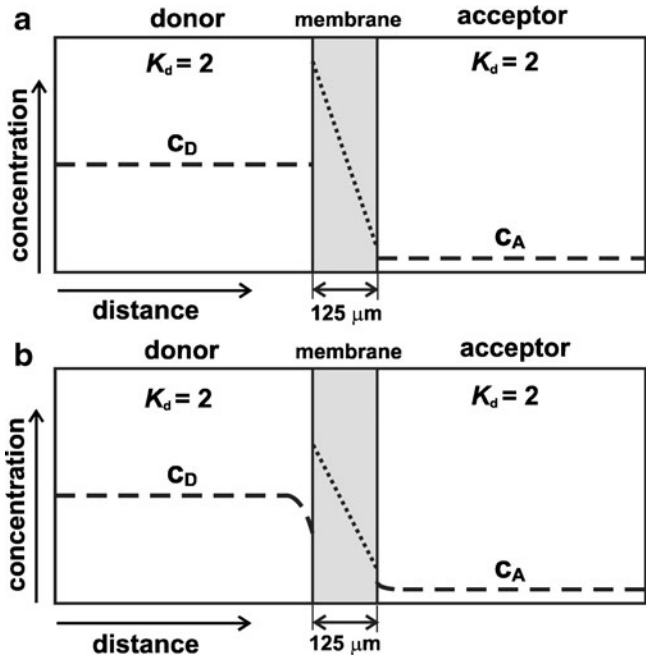

Fig. 2 Schematic diagram of the concentration profile across donor-membrane-acceptor tri-layer for the case of (a) zero UWL thickness, (b) non-zero UWL thickness. The distribution coefficient between the membrane and both donor and acceptor, $K_{\mathrm{d}} = 2$. Linear concentration distribution is assumed within the membrane, time $>\tau_{LAG}$.

(ii) Diffusive flux at the membrane/donor interface:

$$\mathcal{J}(t) = \frac{-V_{\mathrm{D}}}{A}\frac{dc_{\mathrm{D}}(t)}{dt} \tag{3}$$

(iii) Mass balance:

$$V_{\mathrm{D}}c_{\mathrm{D}}(0) = V_{\mathrm{D}}c_{\mathrm{D}}(t) + V_{\mathrm{A}}c_{\mathrm{A}}(t) + V_{\mathrm{m}}c_{\mathrm{m}}(t) \tag{4}$$

where V_{D}, V_{A} and V_{m} are the volumes of the donor, acceptor and membrane, respectively, A is the membrane area, $c_{\mathrm{D}}(0)$ is the initial bulk solute concentration in the donor compartment and $c_{\mathrm{m}}(t)$ is the time-averaged solute concentration within the membrane.

(iv) Expression for the fractional membrane retention R:

$$R = 1 - \frac{V_{\mathrm{D}}c_{\mathrm{D}}(t) + V_{\mathrm{A}}c_{\mathrm{A}}(t)}{V_{\mathrm{D}}c_{\mathrm{D}}(0)} \tag{5}$$

We assume that for time $>\tau_{\mathrm{LAG}}$, $R = R(\infty) = \text{const}$. By combining Eqs. 4 and 5, we obtain the mass balance equation containing the fractional membrane retention R:

$$V_{\mathrm{D}}c_{\mathrm{D}}(0) = V_{\mathrm{D}}c_{\mathrm{D}}(t) + V_{\mathrm{A}}c_{\mathrm{A}}(t) + RV_{\mathrm{D}}c_{\mathrm{D}}(0) \tag{6}$$

In the case of the ideally stirred system with zero UWL thickness, the effective permeability coefficients can be expressed as follows:

$$P_e^{\mathrm{D}\to\mathrm{A}} = P_m^{\mathrm{D}\to\mathrm{A}} = \frac{D_{\mathrm{m}}K_d^{\mathrm{D}}}{h} \tag{7}$$

$$P_e^{\mathrm{A}\to\mathrm{D}} = P_m^{\mathrm{A}\to\mathrm{D}} = \frac{D_{\mathrm{m}}K_d^{\mathrm{A}}}{h} \tag{8}$$

where D_{m} is the diffusion coefficient of the solute within the membrane, $P_m^{\mathrm{D}\to\mathrm{A}}$ and $P_m^{\mathrm{A}\to\mathrm{D}}$ are the membrane permeability coefficients of a solute for the donor-to-acceptor and acceptor-to-donor flux, respectively, K_d^{D} and K_d^{A} are the solute distribution coefficients between the membrane-donor and membrane-acceptor, respectively, and h is the membrane thickness.

Combining Eqs. 2, 3 and 6, we obtain a linear ordinary differential equation:

$$\frac{dc_{\mathrm{D}}(t)}{dt} + ac_{\mathrm{D}}(t) - b = 0 \tag{9}$$

where

$$a = \frac{AP_{\mathrm{e}}^{\mathrm{D}\to\mathrm{A}}}{V_{\mathrm{D}}}\left(1 + \frac{K_{\mathrm{d}}^{\mathrm{A}}}{K_{\mathrm{d}}^{\mathrm{D}}}\frac{V_{\mathrm{D}}}{V_{\mathrm{A}}}\right) \tag{10}$$

and

$$b = \frac{AP_e^{A\to D}}{V_A} c_D(0)\,(1-R) \tag{11}$$

The differential equation (Eq. 9) can be solved to obtain the analytical solution for time $>\tau_{LAG}$:

$$\ln(k) = -a(t-\tau_{LAG}) \tag{12}$$

where k is a function of the measured solute concentration in the acceptor compartment:

$$k = \frac{c_D(0)\,(1-R) - \frac{b}{a} - \frac{V_A}{V_D} c_A(t)}{c_D(\tau_{LAG}) - \frac{b}{a}} \tag{13}$$

where $c_D(\tau_{LAG})$ is the solute bulk concentration in the donor compartment at time $t = \tau_{LAG}$. Physically, k is the normalised concentration change in the cell, corrected for the effects of membrane retention, asymmetry in permeability and distribution coefficient. From the slope of $\ln(k)$ *vs.* time plot, i.e. the constant a (Eq. 10), one directly obtains the effective permeability value. Note that τ_{LAG} is only a constant of integration, so it could be treated as any time in the course of the experiment where the Eqs. 2–13 hold. In practice τ_{LAG} was chosen as the time at which the function of Eq. 12 starts to exhibit a linear behaviour.

Permeability Terms

Equations 2–13 describe the situation where the UWL thickness is zero and the solute concentration in the bulk donor (acceptor) solution and at the donor-membrane (acceptor-membrane) interface is the same (Fig. 2a). In reality, there is always a contribution of the UWL to the permeation and the bulk solute concentration in the donor compartment is always higher than at donor-membrane interface, as depicted in Fig. 2b (likewise, bulk solute concentration in the acceptor is always lower than acceptor-membrane interface concentration). Therefore, what one measures is the *effective* permeability coefficient, P_e (or the apparent permeability coefficient in case of hidden assumptions, such as no membrane retention of the solute and/or no solute back-flux from acceptor to donor compartment (8, 18)). It is assumed that the effective permeability can be described as the total resistance to passive transport across the tri-layer UWL(donor)-membrane-UWL(acceptor) system and is broken down into two following terms (8, 14):

$$\frac{1}{P_e} = \frac{1}{P_u} + \frac{1}{P_m} \tag{14}$$

where P_u is the combined permeability of both donor and acceptor UWLs and, P_m is the membrane permeability.

Permeability Hydrodynamic Model

Approximate relationships between the UWL permeability and stirring rate have been used in previous Caco-2 and PAMPA studies (14, 30):

$$P_u = K\omega^{\alpha} \tag{15}$$

where ω is the angular velocity of stirring, α is an empirical exponent and K is a function of the aqueous diffusion coefficient of the solute D_{aq}, the aqueous kinematic viscosity v and geometrical factors of the permeation cell. The explicit form for the case of symmetric geometry of the rotating-disk electrode was found by Levich (35). The Levich solution applied to the single UWL permeability yields:

$$P_u = 0.62\, D_{aq}^{2/3}\, \nu^{-1/6}\, \omega^{\alpha} \tag{16}$$

where α is 0.5. The exponent α only has the theoretical value of 0.5 in symmetrical systems. In pharmaceutical applications α is often treated as an empirical value, ranging from 0.7 to 1.0, and usually determined by the best fit in UWL permeability analysis (14, 30, 31). We have therefore used the combination of Eqs. 14 and 15 when determining the membrane permeability from the P_e—ω dependency (36–39):

$$\frac{1}{P_e} = \frac{1}{K\,\omega^{\alpha}} + \frac{1}{P_m} \tag{17}$$

From the extrapolation of this relationship to infinite angular velocity, the membrane permeability value, P_m, can be determined.

The permeation cell used in this work was designed to have the same hydrodynamic properties on both sides of the membrane as the rotating-disk electrode. Preliminary electrochemical experiments were performed to test the effect of distance between the paddle and the membrane on the resultant membrane flux. The hydrodynamics were found to follow the Levich equation for paddle-membrane separations between 5 and 10 mm; hence the experimental separation was kept within this range.

Permeability-pH Dependence

For ionisable compounds, the membrane permeability (P_m) depends on pH. Equation 18 defines the pH-independent intrinsic permeability P_0, i.e. the permeability of the neutral fraction, assuming that the pH-partition hypothesis (40) is valid:

$$P_m = P_0 f_n \tag{18}$$

where f_n is the neutral fraction of the solute. Combining Eqs. 14 and 18 and expressing f_n using the Henderson-Hasselbalch equation (41), we obtain the well-known

relationship between the effective permeability and solution pH:

$$\frac{1}{P_e} = \frac{1}{P_u} + \frac{(10^{\pm(pH-pK_a)} + 1)}{P_0} \quad (19)$$

(The sign in the exponent is + for acids and – for bases.) From the slope of this dependence and knowledge of the solute pK_a, one is able to calculate P_0. Similarly, the intercept yields P_u (14, 18).

Numerical Transport Model

A numerical transport model was constructed using the Comsol Multiphysics 2D diffusion and convection solver. The static permeability model was first modified to reflect the true geometry of the experimental system. This involved making several approximations.

First, it was assumed that the internal structure of the membrane permitted diffusion in all directions equally; this assumption was based on microscopic observations of the membrane that showed it to be composed of interlocking fibers with no obvious order to the structure that would drive mass transport in a specific direction (42). The membrane was treated as an entirely open volume in which the solute had apparent diffusion coefficient, D_m. It was further assumed that the binding process of membrane to glass tube (the boundaries of the compartments) was perfectly executed; the amount of membrane blocked by excess adhesive was, therefore, insignificant, and there was no seepage of solution between the glass and the membrane. It was also assumed that the convection profile in the donor phase could be approximated as a rotating disk, although the convection profile in the real experiment would be constrained at the outer edge by the glass wall of the tube. Another implicit assumption was that the solute concentration within the membrane never reached the solubility limit, given the sub-millimolar aqueous concentrations involved. The membrane was assumed to operate as a sink with respect to the donor phase, in that it was assumed that no reverse mass transport occurred (from membrane to donor phase).

In reality, the mass transport of solute through the membrane would be influenced by a variety of factors, including mean diffusion coefficient, mean path length, path length range, solute-lipid interaction and solute-surface interaction. In the model, these influences are aggregated into an apparent membrane diffusion coefficient.

The membrane-donor and membrane-acceptor boundaries were constructed as in the static membrane case, with

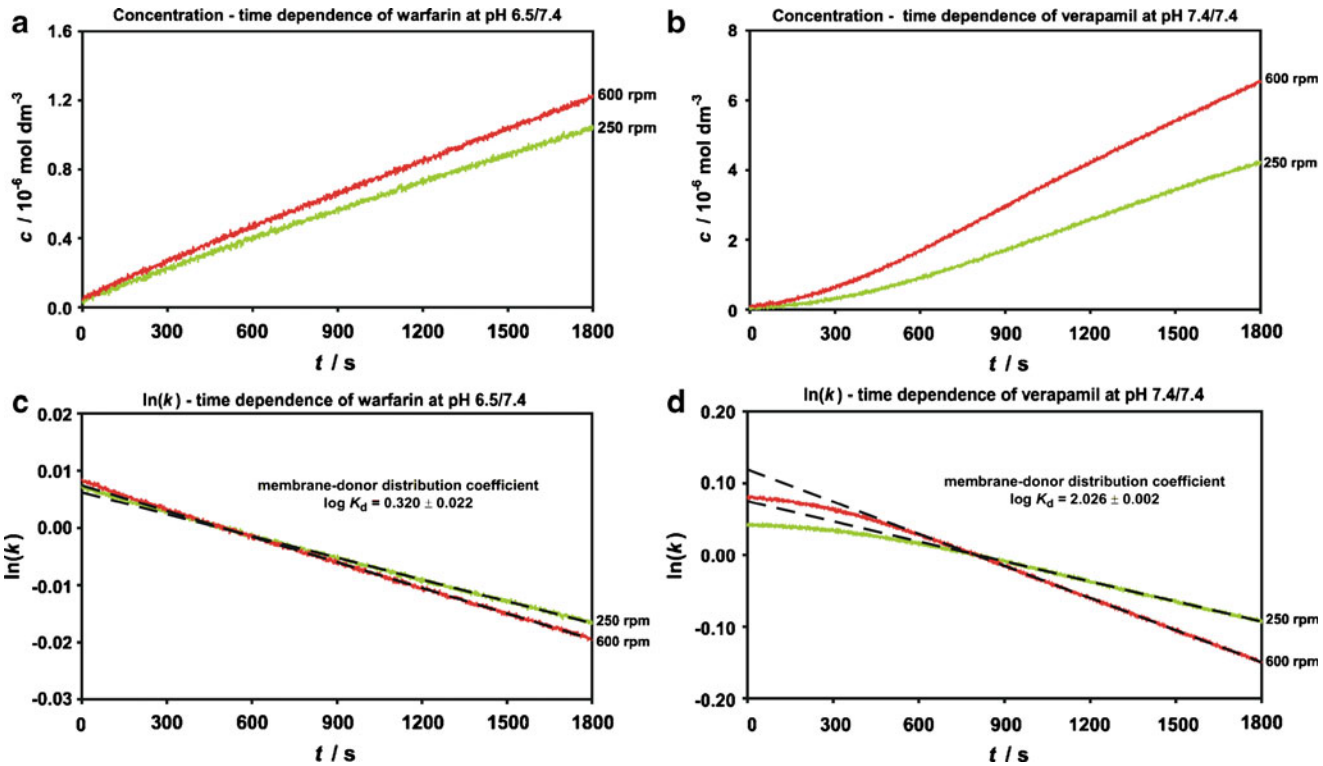

Fig. 3 Example of concentration-time plots for (a) warfarin (309 nm channel) at donor/acceptor pH 6.5/7.4, (b) verapamil (280 nm channel) at donor/acceptor pH 7.4/7.4. The extent of ionisation is roughly the same for the two compounds at these donor pHs. Data for 250 (green) and 600 (red) rpm are shown. Derived ln(*k*)-time plots based on Eq. 12 are shown for (c) warfarin and (d) verapamil. Fitted dashed lines show the linear permeation profile with no membrane loading effects.

the concentrations mapped onto the other side of the interface using an extrusion coupling variable. The direction and extent of flux across the interface were then determined from the respective interfacial concentrations and membrane-donor(acceptor) distribution coefficients. In this case, the distribution coefficients were assumed to be different in each phase, as by controlling the pH of the donor and acceptor phases, the ionisation of the solute will be altered. The distribution coefficient values for a given pH were obtained experimentally by the shake-flask method described above.

RESULTS AND DISCUSSION

In Situ Time-Dependent Permeation

The acceptor compartment absorbance (concentration) of the permeating drug was recorded as a function of time and transformed to a ln(k)-time plot according to Eq. 12. Examples of such plots for both warfarin and verapamil are shown in Fig. 3. Both molecules are ionized to approximately the same extent in these cases. The lag-time τ_{LAG}, was chosen as the time at which the function of Eq. 12 starts to exhibit a linear behaviour. The slope (a) of the ln(k)-time function for time $>\tau_{LAG}$ was then used to calculate the effective permeability, P_e, using Eq. 10.

From Fig. 3c–d, it can be seen that warfarin exhibits a more linear ln(k)-time response than verapamil: the plot of the latter only becomes linear in the middle of the time course. The non-linear behaviour of the verapamil permeation is caused by its higher membrane-donor distribution coefficient (lipophilicity) in comparison to warfarin (see Fig. 3c–d). Due to the higher lipophilicity of verapamil and its higher molar mass (slower diffusion), the membrane saturation period, i.e. lag-time, is considerably enhanced. Fig. 4 shows a numerical simulation of the solute concentration in the membrane and donor as a function of time, when the membrane-acceptor transport is blocked. For the warfarin case (Fig. 4a) at 300 s, the membrane has almost reached saturation due to the low membrane-donor distribution coefficient (log $K_d = 0.320 \pm 0.022$) and moderate molar mass (308.33 g mol^{-1}) of warfarin. For verapamil at the same time, (Fig. 4b), the concentration profile within the membrane has not reached saturation, simply because the amount of solute needed for membrane saturation requires a longer period of diffusion because of the higher membrane-donor distribution coefficient (log $K_d = 2.026 \pm 0.002$) and larger size (molar mass 454.60 g mol^{-1}) of verapamil.

The fact that the membrane needs to be saturated to reach steady-state in the donor-membrane-acceptor system has some important consequences. First of all, if all three

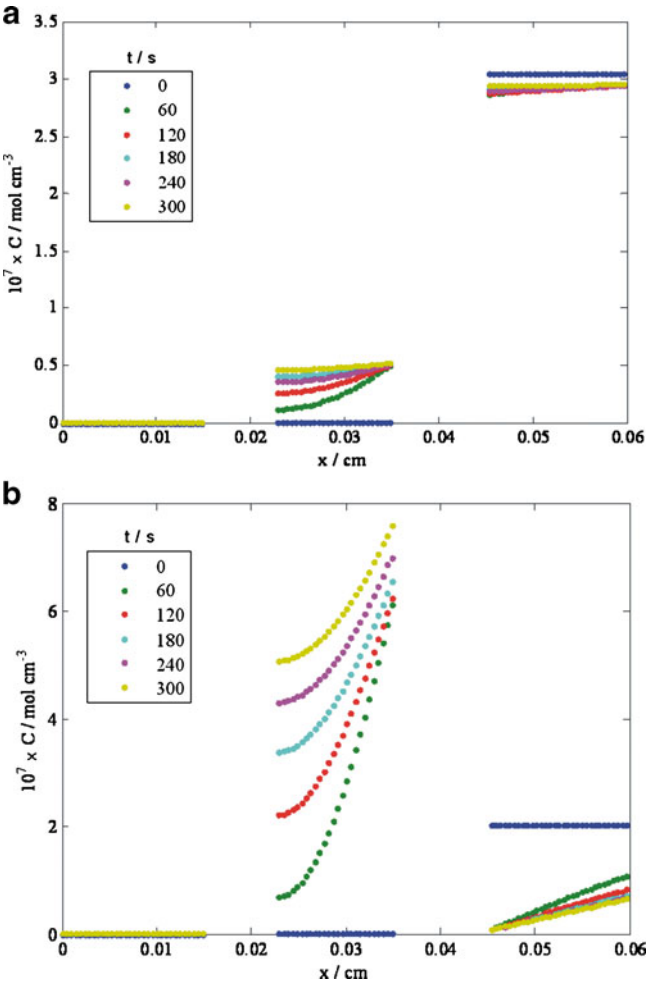

Fig. 4 Numerical simulation of concentration profiles showing membrane saturation with membrane-to-acceptor transport blocked. Left to right: acceptor, membrane, donor. Zero stirring rate. **a** warfarin, with following input parameters: initial donor concentration, $c_D(0) = 3.05 \times 10^{-7}$ mol cm^{-3}, aqueous diffusion coefficient, $D_{aq} = 4.30 \times 10^{-6}$ cm^2 s^{-1}, membrane diffusion coefficient, $D_{mem} = 5.50 \times 10^{-7}$ cm^2 s^{-1}, distribution coefficient (membrane-donor), $K_d = 0.178$. **b** verapamil, with following input parameters: $c_D(0) = 2.02 \times 10^{-7}$ mol cm^{-3}, $D_{aq} = 3.57 \times 10^{-6}$ cm^2 s^{-1}, $D_{mem} = 5.50 \times 10^{-7}$ cm^2 s^{-1}, $K_d = 101.4$

compartments were attached together at the start of the data acquisition, the ln(k)-time profiles would show the same non-linear transient as shown in Fig. 3b and d. During this transient, the time derivative of ln(k) is steadily increasing to reach a constant value at time equal to τ_{LAG}. The length of this transient depends on the lipophilicity and membrane diffusion coefficient of the drug molecule. Higher lipophilicity and/or lower diffusion coefficients would lead to a longer initial transient phase; similarly, lower lipophilicity and/or higher membrane diffusion coefficient shorten the initial transient. Experimentally, however, the three components are never attached at the same time. In our experimental setup, the donor solution is placed in contact with membrane first, with

some 60–120 s elapsing before the acceptor is attached and the experiment is started. For the less lipophilic warfarin molecule, this time is sufficient to saturate the membrane and induce the opposite effect in the transient in order to level down the membrane concentration profile to the steady state shown in Fig. 5a. For the highly lipophilic verapamil molecule, the short pre-acquisition delay of 60–120 s is not sufficient to reach the steady state within the membrane, and a 'normal' transient effect is observed (Fig. 5b). As expected, the experimental lag-time values obtained by fitting the linear and transient segment of ln(k)-time plot increase with membrane-donor distribution coefficient (data shown in Supplementary Material). As a consequence of the transient behaviour, the conventional single time-point analysis, neglecting the lag-time, will lead to underestimation (or, conversely, overestimation) of the effective permeability of lipophilic (hydrophilic) molecules, respectively.

The lag-time also depends of the stirring rate, suggesting that enhanced diffusion across both aqueous sides of the membrane leads to rapid establishment of the steady state across the donor-membrane-acceptor interfaces. The lag-time values for seven different stirring rates in verapamil iso-pH 7.4/7.4 permeation are listed in the Supplementary Material.

Effective Permeability as a Function of Stirring Rate

The effective permeability coefficient was found as a function of the angular velocity of stirring as shown in Fig. 6. The data was analysed assuming that the exponent α (see Eq. 17) had the symmetric geometry value of 0.5 for warfarin and the upper limiting value of 1.0 used in Caco-2 studies for verapamil (31). The intercept of this dependence is the reciprocal of the membrane permeability ($1/P_m$). Using $\alpha = 0.5$ for the verapamil case gave an intercept that fell into the negative region, implying very rapid permeation and breakdown of the ideal hydrodynamics. In order to obtain the membrane permeability coefficient by extrapolation, $\alpha = 1.0$ was used for verapamil (which yields positive intercept values up to pH 8.0).

Permeability-pH Profiles

The effective permeability as a function of stirring rate was measured at different pH values of the donor solution, while keeping the acceptor pH constant (7.4). The permeability-pH profiles that were obtained in this way for both warfarin and verapamil over a wide range of pH values are shown in Fig. 7. The permeation data obtained under hydrodynamic control were supplemented with the unstirred data obtained in the same permeation cell (filled black square symbols in Fig. 7). From the dependence of the effective permeability on pH, Eq. 19, the intrinsic permeability coefficient (P_0) was calculated by least-squares analysis for all the stirring rates shown (0, 250, 400, 600, 1000 and 1500 rpm). The intrinsic permeability was approximately constant for all stirring rates, as expected, and the average value is plotted in Fig. 7 as a black horizontal dashed line. The UWL permeability coefficient, P_u, was calculated separately for each stirring rate using Eq. 19 (dotted horizontal lines in Fig. 7). The membrane

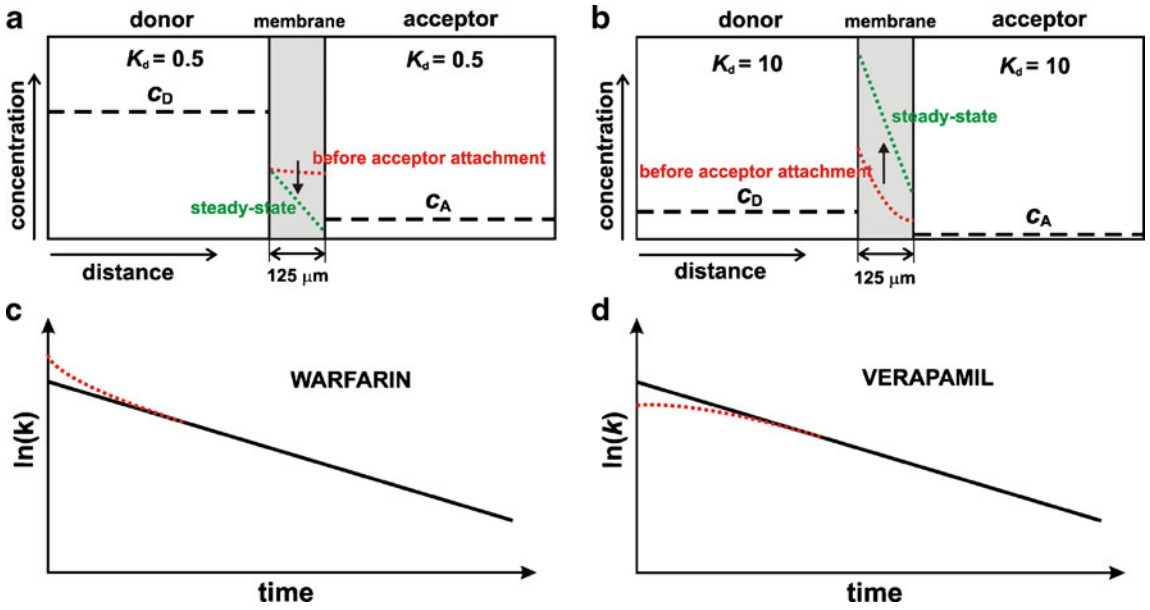

Fig. 5 Schematic diagram of a membrane loading with **a** hydrophilic and **b** lipophilic drug molecule. After the donor solution and membrane are placed in contact, the membrane starts to fill up with the solute (indicated by the red dotted curve). After the acceptor is attached, the concentration within the membrane must (**a**) level down in the warfarin case or (**b**) level up in the verapamil case with steady-state (indicated by the green dotted line). Such membrane pre-loading results in specific transients on ln(k)-time plots shown in **c** warfarin and **d** verapamil.

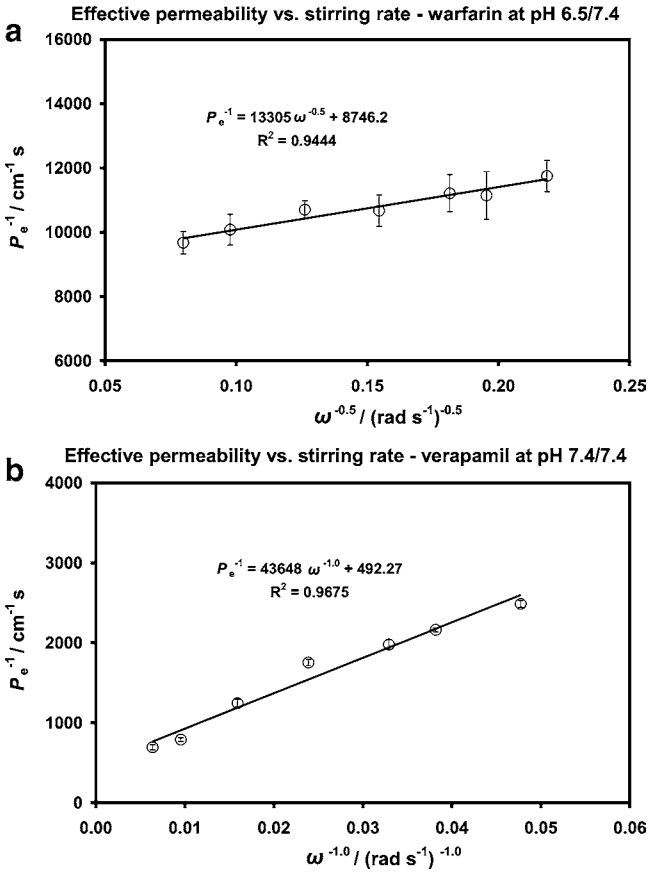

Fig. 6 Dependence of the inverse of effective permeability on the stirring rate for **a** warfarin at pH = 6.5/7.4, **b** verapamil at pH 7.4/7.4. The warfarin and verapamil effective permeability values are plotted against $\omega^{-0.5}$ and $\omega^{-1.0}$, respectively. The membrane permeability is equal to the inverse of the vertical axis intercept. The data points are arithmetic means of three measurements (each being average of four wavelength channels); the error bars are standard deviation of the mean.

permeability coefficient, P_m, calculated from the P_0 value using Eq. 18 is plotted as solid curve in Fig. 7.

The hydrodynamic membrane permeability coefficient extrapolated from the dependence of the effective permeability on stirring rate via Eq. 17 was plotted for each pH as a filled black diamond symbol. Unfilled diamond symbols represent the intrinsic permeability coefficient calculated from the hydrodynamic membrane permeability coefficient. The membrane and intrinsic permeability coefficients obtained from hydrodynamic extrapolation are listed in Table 2 along with the membrane-donor distribution coefficients (determined by shake-flask method), membrane retention (obtained from the mass balance between the donor and acceptor phase) and membrane diffusion coefficients (calculated using Eq. 7). Finally, the hydrodynamic UWL permeability coefficient, P_u, was calculated separately for each stirring rate and pH using Eq. 14 (dashed curves in Fig. 7).

The permeability-pH profile of warfarin is shown in Fig. 7a. Warfarin is a weak acid, with pK_a = 4.82 (8). It is therefore predominantly ionized in the pH range of 6.5–8.0, and there is little change in the effective permeability with stirring rate at this pH. The permeation is membrane-limited in this pH region ($P_u >> P_m$). In the pH range 3.5–6.5, the permeability separation with stirring rate increases, and permeation becomes diffusion-limited, as the aqueous phase permeability becomes comparable with that of the membrane ($P_u \approx P_m$) (6).

Verapamil is a weak base with pK_a = 9.07 (8). The verapamil permeability-pH profile is shown is Fig. 7b for the pH range 5.5–10.0. One can see the overall effective permeability separation with stirring rate is much higher across the whole pH range compared to warfarin. The difference between the unstirred permeability coefficient (filled black squares) value and membrane permeability coefficient is more than 1.7 log units for the common PAMPA condition (donor/acceptor pH 6.5/7.4). The large UWL thickness in the unstirred assay at these pH conditions (3830 μm, calculated using Eq. 20, where D_{aq} is given in Table 1 and P_u is found from Eq. 14):

$$\delta_{UWL} = \frac{D_{aq}}{P_u} \tag{20}$$

makes the assessment of the membrane resistance to permeation impossible. This clearly shows how important the stirring and knowledge of the UWL contribution to permeation is. Although P_u is generally assumed to be constant, the hydrodynamically extrapolated values show a dependence on pH (see the dashed curves on Fig. 7), with P_u falling for both solutes as their degree of ionization increases. The intrinsic permeability values extrapolated from the permeability-stirring rate relationship, Eq. 17, also show a slight dependence on pH (see Fig. 7, unfilled diamond symbols), which is inconsistent with the pH-partition hypothesis (40). In both the warfarin and verapamil cases, the intrinsic permeability increases slightly in the membrane-limited transport region (high pH for warfarin, low pH for verapamil). A possible explanation for this phenomenon is the transport of the ionized solute as ion-pairs, which would increase the intrinsic permeability in the membrane-limited pH region. Ion pairing is likely to be facilitated by the charged organic components within the membrane rather than the aqueous phase counter-ions of low lipophilicity. Ion-pairing mechanisms facilitating permeation/partition were reported in previous literature (43–45). This mechanism could explain the variation in both P_u and P_0.

Further to the permeability measurement, membrane retention defined by Eq. 5 was recorded for both drug molecules. The averaged membrane retention values are listed in Table 2. As expected, membrane retention increases with increasing effective permeability of the drug. The membrane retention was set to zero in cases where the

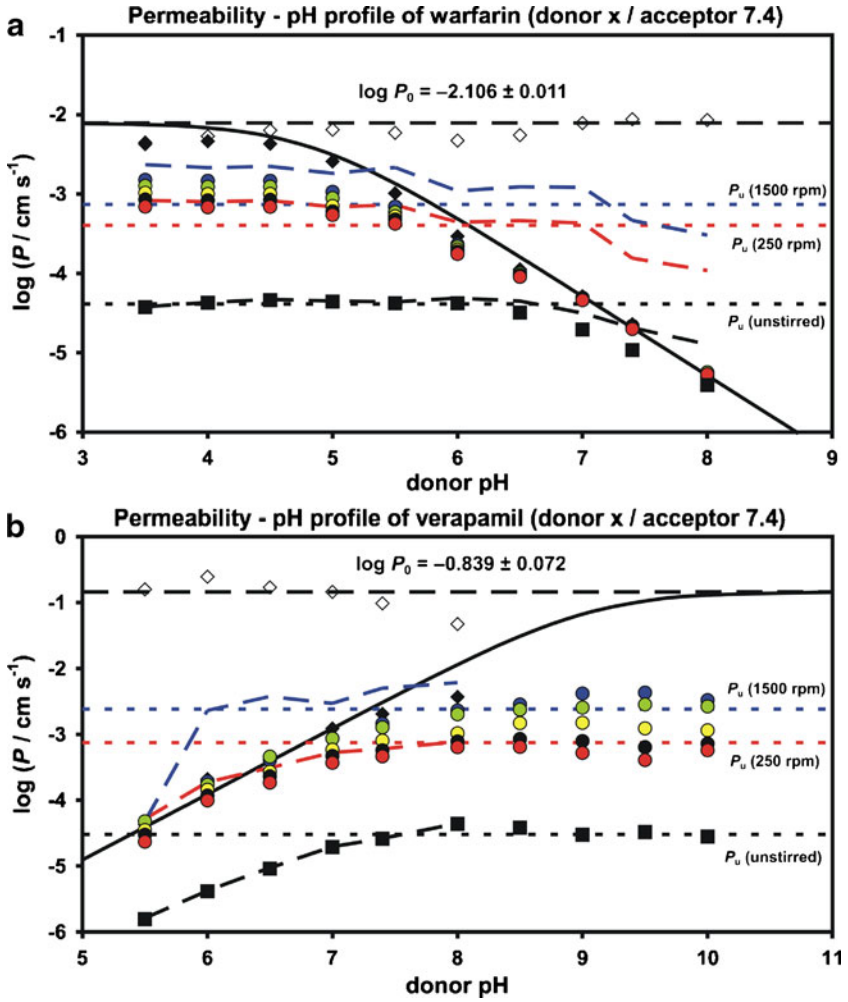

Fig. 7 Permeability-pH profiles of **a** warfarin, **b** verapamil. The marks represent the apparent permeability values at different stirring rates: black square, unstirred; red circle, 250 rpm; black circle, 400 rpm; yellow circle, 600 rpm; green circle, 1000 rpm; blue circle, 1500 rpm. The filled diamond symbols represent the membrane permeability extrapolated from hydrodynamics using Eq. 17 (the exponent α used in this extrapolation was 0.5 for warfarin and 1.0 for verapamil); the unfilled diamond symbols are corresponding intrinsic permeability coefficients calculated using Eq. 18. All data points are arithmetic means of three independent measurements. The error bars are not shown, as their size is comparable or smaller than symbol marks used here. The horizontal dashed lines are UWL permeability values calculated for each stirring rate, using least-square analysis of the permeability-pH dependence, while the dashed curves represent the UWL permeability values extrapolated from the permeability-stirring rate dependence. The uppermost horizontal dashed line is the intrinsic permeability calculated and averaged for all stirring rates, using least-square analysis of Eq. 19. The solid curve represents the membrane permeability calculated from the dashed line using Eq. 18.

calculated value was negative due to experimental error (negative $\%R$ values were not generally lower than −5%).

Permeability Hydrodynamics

According to the hydrodynamic model of permeability described earlier, we have investigated the value of the hydrodynamic exponent α from Eqs. 15–17. The α values reported in literature were obtained as a best-fit of the stirring-based analysis of UWL permeability. The exponent varied from 0.709 (14) in PAMPA studies to 0.8 (30) and 1.0 (31) in Caco-2 studies. In fact, the exponent α is dependent on the membrane permeability, and its value varies with solute identity and assay pH. Plotting the effective permeability against angular velocity in log-log units yields α as a gradient. Fig. 8 shows the dependence of α on donor pH. It increases with increasing neutral fraction both for warfarin and verapamil. Comparing the data in Fig. 8 with Fig. 7, it is evident that α is a measure of the effective permeability separation with stirring rate. As expected, for warfarin, α increases to its limiting value of 0.5 in the diffusion-limited low pH region. The verapamil data, however, suggest non-standard hydrodynamic behaviour with α value exceeding 1.0 at high pH.

The hydrodynamic behaviour of verapamil permeation at donor/acceptor pH 7.4/7.4 was investigated using a

Table 2 Permeability coefficients, membrane retentions, membrane-donor distribution coefficients and membrane diffusion coefficients of warfarin and verapamil (The values are means of three independent measurements; the errors standard deviation of the means.)

donor pH	log (P_m /cms^{-1})[a]	log (P_0 /cms^{-1})[b]	%R [c]	log K_d[d]	D_m / 10^{-6}cm^{2}s^{-1} [e]
Warfarin					
3.5	−2.372 ± 0.002	−2.352 ± 0.002	4.6 ± 0.7	1.809 ± 0.015	0.825 ± 0.036
4.0	−2.334 ± 0.003	−2.373 ± 0.003	0.4 ± 0.7	1.790 ± 0.009	0.939 ± 0.045
4.5	−2.368 ± 0.003	−2.198 ± 0.003	4.1 ± 1.6	1.716 ± 0.001	1.030 ± 0.019
5.0	−2.590 ± 0.009	−2.190 ± 0.009	6.2 ± 2.8	1.277 ± 0.025	1.698 ± 0.113
5.5	−2.991 ± 0.003	−2.229 ± 0.003	4.0 ± 1.3	1.079 ± 0.011	1.065 ± 0.067
6.0	−3.534 ± 0.008	−2.326 ± 0.008	1.5 ± 0.6	0.619 ± 0.009	0.879 ± 0.078
6.5	−3.948 ± 0.019	−2.259 ± 0.019	0.0 ± 0.1	0.320 ± 0.022	0.674 ± 0.091
7.0	−4.289 ± 0.040	−2.106 ± 0.040	0.0 ± 0.0	−0.303 ± 0.024	1.290 ± 0.449
7.4	−4.640 ± 0.027	−2.059 ± 0.027	0.9 ± 0.7	−0.750 ± 0.029	1.611 ± 0.164
8.0	−5.249 ± 0.030	−2.069 ± 0.030	0.0 ± 0.0	−1.506 ± 0.084	2.258 ± 0.055
Verapamil					
5.5	−4.372 ± 0.016	−0.802 ± 0.016	0.0 ± 0.0	0.582 ± 0.037	0.139 ± 0.000
6.0	−3.679 ± 0.014	−0.609 ± 0.014	0.2 ± 0.2	0.994 ± 0.005	0.266 ± 0.001
6.5	−3.341 ± 0.035	−0.770 ± 0.035	2.1 ± 0.7	1.428 ± 0.008	0.213 ± 0.002
7.0	−2.912 ± 0.010	−0.838 ± 0.010	6.9 ± 1.3	1.825 ± 0.005	0.215 ± 0.002
7.4	−2.692 ± 0.007	−1.013 ± 0.007	6.1 ± 1.7	2.026 ± 0.002	0.239 ± 0.006
8.0	−2.433 ± 0.005	−1.328 ± 0.005	10.8 ± 1.8	2.426 ± 0.024	0.173 ± 0.007
8.5	–	–	16.3 ± 3.7	2.558 ± 0.013	–
9.0	–	–	16.6 ± 3.3	2.718 ± 0.026	–
9.5	–	–	20.1 ± 3.1	3.017 ± 0.044	–
10.0	–	–	10.7 ± 2.5	3.114 ± 0.050	–

[a] Membrane permeability coefficient determined from hydrodynamic extrapolation

[b] Intrinsic permeability coefficient calculated using Eq. 18

[c] Membrane retention calculated using Eq. 5

[d] Membrane-donor phase distribution coefficient determined by shake-flask method

[e] Membrane diffusion coefficient calculated using Eq. 7

reduced apparent membrane area (0.1 cm^2) on the donor side. One possible explanation for the deviation of α from the hydrodynamic limit of 0.5 was the difference in the hydrodynamics from the conventional rotating-disk configuration. In the case studied here, the apparent membrane area occupies the whole face of the donor compartment (see Fig. 1). Consequently, if this factor were significant, reducing the apparent membrane area should bring α to 0.5 (or lower, depending on the system pH, see above). Both the effective permeability coefficients and α values obtained from the standard and reduced membrane area experiment were, however, almost identical (see Supplementary Material), indicating that the discrepancy seen with verapamil is not due to the hydrodynamics of the cell. Hence, a preliminary explanation of the atypical hydrodynamic behaviour of verapamil can be found in its high lipophilicity and correspondingly high permeability value.

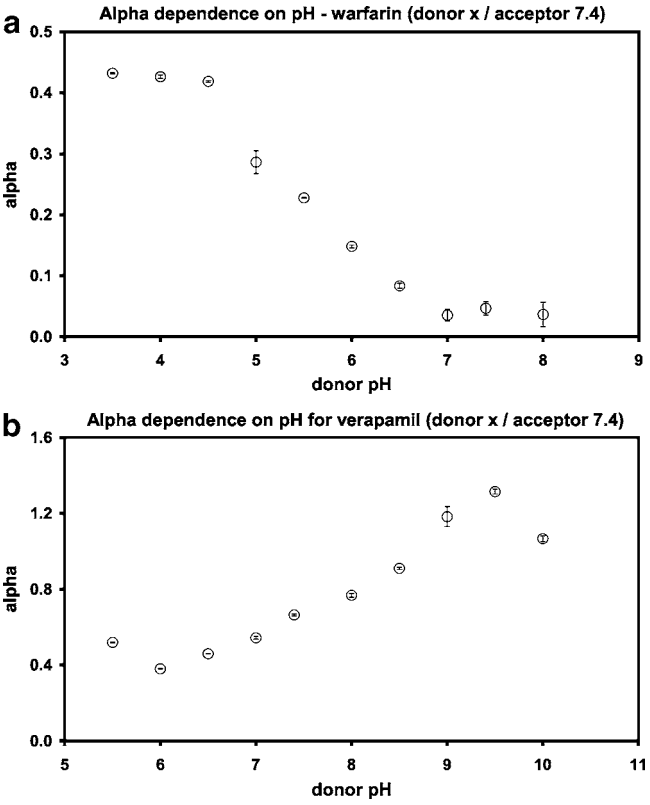

Fig. 8 Hydrodynamic exponent α calculated by least-square analysis of log P_e – log ω dependence for **a** warfarin, **b** verapamil. The error bars are standard deviations calculated from the least-square analysis error

CONCLUSIONS

The permeability of drug molecules has been investigated in a PAMPA configuration using a time-dependent approach: to the best of our knowledge, this is the first report using such an *in situ* analysis. The use of an *in situ* permeability measurement, coupled with controlled hydrodynamics, allows the accurate measurement of intrinsic permeability and has

revealed that a significant lag time exists before a steady membrane transport rate is established. The lag time is strongly correlated with the lipophilicity of the solute, leading to differing initial forms of the concentration transient. Failure to account for this lag time leads to an underestimation of permeability for lipophilic molecules (and, conversely, permeability overestimation for hydrophilic molecules), which is potentially a significant problem for PAMPA, given the current focus in the pharmaceutical industry on target molecules of increasing lipophilicity. The effect of unstirred water layer permeability on the effective permeability has been clearly revealed by the use of the hydrodynamic (rotating) system. Measurement of permeability as a function of pH and stirring rate gives an apparent pH dependence of the membrane permeability, from which we infer that some transport of ionized solutes occurs, most likely via an ion-pairing mechanism. The hydrodynamics of the rotating disk describe the permeability of the moderately lipophilic molecule (warfarin) well, but deviations are seen for the highly lipophilic solute (verapamil). Ongoing work is studying the transport dependence of permeability for a larger set of model drug compounds.

ACKNOWLEDGEMENTS

We thank our industrial collaborator, AstraZeneca, and EPSRC for funding and Dr. J. Matthew Wood (AstraZeneca, Alderley Park) for consultation and training in the industrial PAMPA method.

REFERENCES

1. Fade V. Link between drug absorption solubility and permeability measurements in Caco-2 cells. J Pharm Sci. 1998;87:1604–7.
2. Artursson P, Karlsson J. Correlation between oral drug absorption in humans and apparent drug permeability coefficients in human intestinal epithelial (CACO-2) cells. Biochem Biophys Res Commun. 1991;17:880–5.
3. Irvine JD, Takahashi L, Lockhart K, Cheong J, Tolan JW, Selick HE *et al.* MDCK (Madin-Darby canine kidney) cells: a tool for membrane permeability screening. J Pharm Sci. 1999;88:28–33.
4. Galinis-Luciani D, Nguyen L, Yazdanian M. Is PAMPA a useful tool for discovery? J Pharm Sci. 2007;96:2886–92.
5. Avdeef A, Bendels S, Di L, Faller B, Kansy M, Sugano K *et al.* PAMPA - Critical factors for better predictions of absorption. J Pharm Sci. 2007;96:2893–909.
6. Avdeef A. The rise of PAMPA. Expert Opin Drug Metab Toxicol. 2005;1:325–42.
7. Mälkia A, Murtomäki L, Urtti A, Kontturi K. Drug permeation in biomembranes: *In vitro* and in silico prediction and influence of physicochemical properties. Eur J Pharm Sci. 2004;23:13–47.
8. Avdeef A. *Absorption and Drug Development: Solubility, Permeability, and Charge State*, Wiley-Interscience, 2003.
9. Avdeef A. High-throughput measurement of permeability profiles, *Drug Bioavailability*, Wiley-VCH Weinheim, 2003.
10. Kansy M, Senner F, Gubernator K. Physicochemical high throughput screening: parallel artificial membrane permeation assay in the description of passive absorption processes. J Med Chem. 1998;41:1007–10.
11. Kansy M, Fischer H, Kratzat K, Senner F, Wagner B, and Parilla I. High-Throughput Artificial Membrane Permeability Studies in Early Lead Discovery and Development, *Pharmacokinetic Optimization in Drug Research*. Helvetic Chim Acta. 2001.
12. Avdeef A, Strafford M, Block E, Balogh MP, Chambliss W, Khan I. Drug absorption *in vitro* model: Filter-immobilized artificial membranes: 2. Studies of the permeability properties of lactones in Piper methysticum Forst. Eur J Pharm Sci. 2001;14:271–80.
13. Bermejo M, Avdeef A, Ruiz A, Nalda R, Ruell JA, Tsinman O *et al.* PAMPA - a drug absorption *in vitro* model 7. Comparing rat *in situ*, Caco-2, and PAMPA permeability of fluoroquinolones. Eur J Pharm Sci. 2004;21:429–41.
14. Avdeef A, Nielsen PE, Tsinman O. PAMPA - A drug absorption *in vitro* model: 11. Matching the *in vivo* unstirred water layer thickness by individual-well stirring in microtitre plates. Eur J Pharm Sci. 2004;22:365–74.
15. Sugano K, Hamada H, Machida M, Ushio H, Saitoh K, Terada K. Optimized conditions of bio-mimetic artificial membrane permeation assay. Int J Pharm. 2001;228:181–8.
16. Sugano K, Nabuchi Y, Machida M, Aso Y. Prediction of human intestinal permeability using artificial membrane permeability. Int J Pharm. 2003;257:245–51.
17. Sugano K, Takata N, Machida M, Saitoh K, Terada K. Prediction of passive intestinal absorption using bio-mimetic artificial membrane permeation assay and the paracellular pathway model. Int J Pharm. 2002;241:241–51.
18. Wohnsland F, Faller B. High-throughput permeability pH profile and high-throughput alkane/water log P with artificial membranes. J Med Chem. 2001;44:923–30.
19. Faller B, Grimm HP, Loeuillet-Ritzler F, Arnold S, Briand X. High-throughput lipophilicity measurement with immobilized artificial membranes. J Med Chem. 2005;48:2571–6.
20. Chen X, Murawski A, Patel K, Crespi CL, Balimane PV. A novel design of artificial membrane for improving the PAMPA model. Pharm Res. 2008;25:1511–20.
21. Flaten GE, Skar M, Luthman K, Brandl M. Drug permeability across a phospholipid vesicle based barrier: 3. Characterization of drug-membrane interactions and the effect of agitation on the barrier integrity and on the permeability. Eur J Pharm Sci. 2007;30:324–32.
22. Flaten GE, Dhanikula AB, Luthman K, Brandl M. Drug permeability across a phospholipid vesicle based barrier: a novel approach for studying passive diffusion. Eur J Pharm Sci. 2006;27:80–90.
23. Flaten GE, Bunjes H, Luthman K, Brandl M. Drug permeability across a phospholipid vesicle-based barrier. 2. Characterization of barrier structure, storage stability and stability towards pH changes. Eur J Pharm Sci. 2006;28:336–43.
24. Di L, Kerns EH, Fan K, McConnell OJ, Carter GT. High throughput artificial membrane permeability assay for blood-brain barrier. Eur J Med Chem. 2003;38:223–32.
25. Przybylo M, Olzynska A, Han S, Ozyhar A, Langner M. A fluorescence method for determining transport of charged compounds across lipid bilayer. Biophys Chem. 2007;129:120–5.
26. Gjelstad A, Rasmussen KE, Pedersen-Bjergaard S. Electrokinetic migration across artificial liquid membranes. Tuning the membrane chemistry to different types of drug substances. J Chrom. 2006;1124:29–34.
27. Balon K, Riebesehl BU, Müller BW. Drug liposome partitioning as a tool for the prediction of human passive intestinal absorption. Pharm Res. 1999;16:882–8.

28. Seo PR, Teksin ZS, Kao JPY, Polli JE. Lipid composition effect on permeability across PAMPA. Eur J Pharm Sci. 2006;29:259–68.
29. Avdeef A, Artursson P, Neuhoff S, Lazorova L, Gråsjö J, Tavelin S. Caco-2 permeability of weakly basic drugs predicted with the Double-Sink PAMPA pKa flux method. Eur J Pharm Sci. 2005;24:333–49.
30. Adson A, Burton PS, Raub TJ, Barsuhn CL, Audus KL, Ho NFH. Passive diffusion of weak organic electrolytes across Caco-2 cell monolayers: Uncoupling the contributions of hydrodynamic, transcellular, and paracellular barriers. J Pharm Sci. 1995;84:1197–204.
31. Karlsson J, Artursson P. A method for the determination of cellular permeability coefficients and aqueous boundary layer thickness in monolayers of intestinal epithelial (Caco-2) cells grown in permeable filter chambers. Int J Pharm. 1991;71:55–64.
32. Lennernäs H. Human intestinal permeability. J Pharm Sci. 1998;87:403–10.
33. Molloy BJ, Tam KY, Wood JM, Dryfe RAW. A hydrodynamic approach to the measurement of the permeability of small molecules across artificial membranes. Analyst. 2008; 133:655–9.
34. Mayer PT, Anderson BD. Transport across 1, 9-decadiene precisely mimics the chemical selectivity of the barrier domain in egg lecithin bilayers. J Pharm Sci. 2002;91:640–6.
35. Levich VG. Physicochemical hydrodynamics. London: Englewood Cliffs; 1962.
36. Albery WJ, Burke JF, Leffler EB, Hadgraft J. Interfacial transfer studied with a rotating diffusion cell. J Chem Soc Faraday Trans I. 1976;72:1618–26.
37. Guyand RH, Honda DH. Solute transport resistance at the octanol - water interface. Int J Pharm. 1984;19:129–37.
38. Leahy DE, Wait AR. Solute transport resistance at water-oil interfaces. J Pharm Sci. 1986;75:1157–61.
39. Amidon GE, Higuchi WI, Ho NFH. Theoretical and experimental studies of transport of micelle-solubilized solutes. J Pharm Sci. 1982;71:77–84.
40. Shore PA, Brodie BB, Hogben CAM. The gastric secretion of drugs - a pH partition hypothesis. J Pharmacol Exp Ther. 1957;119:361–9.
41. Atkins P, de Paula J. Physical chemistry for the life sciences. Oxford University Press, 2006.
42. Charcosset C, Bernengo JC. Comparison of microporous membrane morphologies using confocal scanning laser microscopy. J Membr Sci. 2000;168:53–62.
43. Sarveiya V, Templeton JF, Benson HAE. Ion-pairs of ibuprofen: Increased membrane diffusion. J Pharm Pharmacol. 2004;56:717–24.
44. Takacs-Novak K, Szasz G. Ion-pair partition of quaternary ammonium drugs: the influence of counter ions of different lipophilicity, size, and flexibility. Pharm Res. 1999;16:1633–8.
45. Neubert R. Ion pair transport across membranes. Pharm Res. 1989;6:743–7.
46. Dollery CT. Therapeutic drugs. Churchill Livingstone, 1999.
47. Obach RS, Lombardo F, Waters NJ. Trend analysis of a database of intravenous pharmacokinetic parameters in human for 670 drug compounds. Drug Metab Dispos. 2008;36:1385–405.